Charge Transfer Dynamics between Cesium Lead Halide Perovskite Nanocrystals and Surface Anchored Naphthalimide Acceptor

Meng Li,[a,b] Silvano R. Valandro,[b] Ru He,[b] Yan Zhao[b],

Ping Yang[a*] and Kirk S. Schanze[b*]

[a] School of Material Science & Engineering, University of Jinan, Jinan, 250022, P. R. China, E-mail: mse_yangp@ujn.edu.cn

[b] Department of Chemistry, University of Texas at San Antonio, San Antonio, Texas 78249, United States, E-mail: kirk.schanze@utsa.edu

ABSTRACT

A series of 1,8-naphthalimide (NI) electron acceptors with a primary amine functional group linked to the N-position of the imide by -$(CH_2)_n$- linkers with varying length are found to quench the photoluminescence (PL) of $CsPbBr_3$ nanocrystals (NC). Three NI-based quenchers were explored, NI-1, NI-2, NI-3, with n = 2, 8, and 12, respectively. The PL quenching is attributed to photoinduced electron transfer from the exciton state of the $CsPbBr_3$ NCs to the naphthylimide acceptor. An NI acceptor that lacks the NH_2 group does not quench the PL, which reveals that the amino group serves to anchor the acceptors to the surface of the NC. The photoinduced charge transfer mechanism is supported by picosecond transient absorption (TA), which finds a long-lifetime bleach (> 7 ns) for the $CsPbBr_3$ NCs with surface anchored NI-1 acceptor. Steady state and time resolved PL quenching was subjected to Stern-Volmer (SV) analysis. The results show that the quenching efficiency varies in the order NI-1 >> NI-2 > NI-3, with K_{SV} ranging from ~ 10^6 M^{-1} for NI-1 to ~10^5 M^{-1}

for NI-3. The quenching efficiency is approximately the same for steady-state and dynamic quenching. The results are interpreted by a mechanism where the exciton quenching dynamics are controlled by the rate of interfacial electron transfer. Diffusion and/or detrapping of the $CsPbBr_3$ exciton may also play a role in determining the rate of quenching.

Introduction

In the last few decades, lead halide perovskites with the formula ABX_3 ($A = Cs^+/CH_3NH_3^+$; B = Pb; $X = Cl^-/Br^-/I^-$) have drawn enormous attention because of their outstanding optical properties, such as broad absorption spectra, high emission quantum yields, and narrow, symmetric and tunable emission spectra throughout the entire visible spectrum.[1-2] With these attractive optical properties, perovskites have shown great potential in many fields including solar cells, photovoltaics, light-emitting diodes, and lasers.[2-3] Owing to their controllable bandgaps and weak exciton binding energy, lead halide perovskites have achieved significant improvements as light harvesters in solid-state solar cells. In theory, the efficiency of $CsPbI_3$ perovskite-based solar cells can reach as high as 21.7%.[4]

All-inorganic cesium lead halide perovskite ($CsPbX_3$, X = Cl, Br, and I) nanocrystals (NCs), which have high photoluminescence quantum yields and stability, have received attention in perovskite-based photovoltaic systems.[5-6] Not only determined by the excellent light harvesting ability of perovskite materials, the conversion efficiency of their photovoltaic devices is also related to the charge transfer (CT) efficiency between light harvesters and hole/electron transporting materials. Electron donating, accepting and charge transporting materials, which are sandwiched with the perovskite light harvesters, play an important role for extraction of charge carriers from the active layer and decrease exciton recombination.[7] To

achieve higher photovoltaic conversion efficiency, the detailed understanding of CT process across the interface and engineering interfacial energy-level alignment is necessary. Besides, the CT process could endow perovskites with new photoproperties, such as wider absorption spectrum, or novel emission properties.[8] Nevertheless, the interfacial CT process and ultrafast exciton dynamics between all-inorganic $CsPbX_3$ NCs and molecular acceptors have not been fully investigated.[8-12] All-inorganic $CsPbX_3$ NCs have significant potential in optoelectronic devices and photocatalytic applications if their interfacial charge transfer dynamics can be fully understood.[12-13]

1,8-Naphthalimide (NI), a moderate electron acceptor, is also the core structure of several noteworthy molecular acceptors, such as naphthalenediimide, perylenediimide, and terrylenediimide.[14-15] It has been demonstrated that NI possess great potential for applications such as dye lasers, photoluminescent (PL) thin films, fluorescent chemical sensors and fluorescent molecular switches.[16] Recently, NI-functionalized fullerenes were applied for perovskite-based solar cells because their LUMO energy level gives rise to a higher open-circuit voltage (V_{oc}).[17-18] Solar cells with photovoltaic conversion efficiency of 3.6% and 7.64% have been fabricated that are based on NI electron acceptors.[19-20]

Here, the series of naphthalene imides shown in Chart 1 was used as electron acceptors linked to the surface of all inorganic $CsPbBr_3$ NCs. The dynamics of CT from $CsPbBr_3$ NCs to the NI acceptors were investigated. The NI moiety is functionalized with a primary amine group which serves as an anchor to the surface of the $CsPbBr_3$ NCs; control studies reveal that the amine linker is critical to allow the electron transfer process between the $CsPbBr_3$ NCs and the NI moiety. Our results give insight concerning the mechanism and dynamics of interfacial electron transfer.

The ability to dissociate excitons in perovskites by connecting with an organic semiconductor in a donor/acceptor configuration will provide a new prospect to increase the efficiency of light-harvesting and light-emitting applications for all inorganic perovskites.

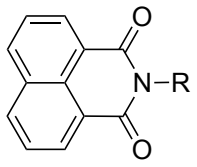

NI : R = -$CH_2CH_2CH_3$
NI-1 : R = -$(CH_2)_2$-NH_2
NI-2 : R = -$(CH_2)_8$-NH_2
NI-1 : R = -$(CH_2)_{12}$-NH_2

Chart 1. Structures of NI series

Experimental Section

Chemicals. Lead (II) bromide ($PbBr_2$, 99.999%), cesium carbonate (Cs_2CO_3, 99.9%), Lead (II) iodide (PbI_2, 98%), octadecene (ODE, technical grade of 90%), oleic acid (OA, 99%), oleylamine (OAm, 70%) were purchased from Sigma-Aldrich. Solvents were purchased as anhydrous or dried by elution through an MBruan MB-SPS-800 solvent purification system. 1,8-Naphthalic anhydride (CAS: 81-84-5), 1,2-diaminoethane (107-15-3), propylamine (107-10-8), 1,8-diaminooctane (373-44-4), 1,12-dodecanediamine were purchased from Sigma-Aldrich.

Synthesis of $CsPbBr_3$ NCs. A typical hot-injection method with some modification was used to prepare $CsPbBr_3$ NCs.[1] Cesium oleate (Cs-OA) precursor solutions, Cs_2CO_3 (0.16 g) and OA (2.5 mL) along with ODE (6 mL) were added into a 50 mL 3-neck flask. The temperature of the solution was kept at 120 ^oC for 30 min and then increased to 150 ^oC under N_2 to completely dissolve Cs_2CO_3. For preparing $CsPbBr_3$ NCs, ODE (5 mL) and of $PbBr_2$ (0.188 mmol) salt were loaded into a 4-neck flask. The solution was purged using N_2 at 120 °C for 1 h before the injection of OAm (1 mL) and OA (1 mL). Prolonging the reaction time allowed the $PbBr_2$ salt to dissolve completely. And then, the temperature was raised to 180 ^oC, with the

immediately injection of Cs–OA precursor solution (0.4 mL). The reaction was terminated by immersion of the reaction vessel in an ice bath within 10 s. To purify the synthesized samples, the cooled solution was centrifuged at 9000 rpm for 4 min to remove unreacted ligands. After that, hexane was added to disperse the precipitate. Centrifugation was repeated at 4000 rpm for 4 min to remove aggregated NCs. By changing the volume of hexane, $CsPbBr_3$ stock solutions with different concentrations were prepared. The concentration of the $CsPbBr_3$ stock solution was calculated from the absorption at 400 nm as described in the Supporting Information. Throughout the paper concentration refers to $CsPbBr_3$ nanoparticle concentration.

Synthesis of NI Series. The series of NI acceptors (NI and NI-n) were synthesized by using the same procedures described in the literature with slight modifications (Figure S2).[21] For NI-n, 10.1 mmol of 1,8-naphthalic anhydride was added into 100 mL of ethanol along with 68 mmol of 1,2-diaminoethane, 1,8-diaminooctane or 1,12-dodecanediamine. For NI, all the experimental conditions were the same, except for 18 mmol of propylamine was used. It took 6 h to reflux the mixture. After cooling the reaction, the solvent was evaporated under reduced pressure. The resulting solid was purified by silica gel chromatography (DCM/Methanol 1:3) to afford NI series as white powders. ^{1}H-NMR spectra of the series of compounds are shown in Figure S3 (ESI†). Acetone was selected as the solvent for NI series compound due to the good solubility for the compounds and compatibility with the $CsPbBr_3$ NCs (Figure S4, ESI†).

Synthesis of $CsPbBr_3$-NI-n (n = 1, 2, 3) Hybrids. By adding 50 μL of $CsPbBr_3$ stock solution into 2 mL hexane, the $CsPbBr_3$ solution was diluted to 0.04 μM. $CsPbBr_3$-NI-n (n=1, 2, 3) hybrids were prepared by adding an acetone solution of NI-n into the diluted $CsPbBr_3$ stock solution (0.04 μM) without further purification. For morphology and structure characterization, as well as steady state measurements, 10 μL of NI-n solution (0.4 mM) was added into 2 mL $CsPbBr_3$ solution (0.04 μM). For the transient absorption measurements, the concentration of $CsPbBr_3$ solution was 1.54 μM. For the $CsPbBr_3$-NI-1 hybrid, excess NI-1 solid was added into the $CsPbBr_3$ hexane solution, and then the unreacted NI-1 solid was removed by centrifugation. Because of the poor solubility of NI-1 in hexane, only surface anchored NI-1 remained in the final solution. For the Stern-Volmer quenching experiments, NI-n solution was gradually added into 2 mL of $CsPbBr_3$ solution (0.04 μM). The concentration of NI-n in the mixture was increased from 0 μM to 2 μM. To demonstrate the critical role of amino group, 10 μL NI solution (0.4 mM) was added into 2 mL $CsPbBr_3$ stock solution (0.04 μM).

Structural Characterization. A JEM-2100F microscope operated at 200 kV recorded the high-resolution transmission electron microscopy (HRTEM) images. The X-ray scattering was carried out on a Bruker D8 X-ray powder diffractometer (XRD). Thermo Scientific K-Alpha Al−Kα X-ray source was used in X-ray photoelectron spectroscopy (XPS) analysis. ^1H nuclear magnetic resonance (NMR) spectra were measured on a 500 MHz Bruker Advance III HD spectrometer using tetramethylsilane (TMS) as internal standard and chloroform-D ($CDCl_3$) as the solvent. Fourier transform infrared (FTIR) spectra were measured with an FTIR spectrometer (Thermo Electron, Nicolet 380).

Steady State and Time-Resolved PL Measurements. Absorption and photoluminescence spectra were measured on Shimadzu UV-2600 spectrophotometer and Edinburgh FLS 1000 photoluminescence spectrometer, respectively. Photoluminescence quantum yields were measured on an Edinburgh FLS 1000 photoluminescence spectrometer equipped with SM4 Integrating sphere. Fluorescence lifetimes were measured using PicoQuant FluoTime 300 fluorescence lifetime spectrophotometer by time-correlated single photon counting.

Transient Absorption Measurements. Femtosecond-picosecond transient absorption (TA) spectroscopy was carried out as previously described.[22]

Results and Discussion

Figure 1a shows the steady-state absorption spectra of $CsPbBr_3$ NCs, NI-1, and the $CsPbBr_3$-NI-1 hybrid sample that is prepared by addition of excess NI-1 to a solution of the $CsPbBr_3$ nanoparticles. The comparison in Fig. 1a reveals that the absorption of the $CsPbBr_3$-NI-1 hybrid sample exhibits the features characteristic of the nanoparticles, namely the exciton absorption with peak at 509 nm and broad absorption at shorter wavelengths, along with the superimposed near-UV absorption bands at 310 - 360 nm due to NI-1. The $CsPbBr_3$ nanoparticles exhibit an efficient characteristic photoluminescence (PL) at 520 nm. Addition of excess NI-1 to a solution of $CsPbBr_3$ leads to rapid quenching of the luminescence as shown in Figure 1b. The results illustrate that NI-1 induces dramatic PL quenching, which suggests an efficient interaction between the $CsPbBr_3$ exciton and NI-1 that leads to non-radiative decay. The color images in Figure 1b reveal that the luminescence of $CsPbBr_3$ is almost totally quenched within 30 s following addition of NI-1. The PL quantum efficiency of $CsPbBr_3$ and the $CsPbBr_3$-NI-1 hybrid were measured to be 93% and 1%, respectively; this shows that addition of excess NI-1 nearly completely quenches the

$CsPbBr_3$ exciton. The quenching in the PL spectra confirmed the NI-1 moiety is anchored on the surface of $CsPbBr_3$ NCs presumably due to a specific interaction between the primary amino group ($-NH_2$) and the surface of the $CsPbBr_3$ NCs.[23-25] In order to confirm that the amino group is essential in anchoring the imide electron acceptor on the NC surface, a control experiment was carried out to examine the effect of addition of NI, which lacks the NH_2 group (Chart 1), on the $CsPbBr_3$ NC emission. This experiment shows that addition of a comparable amount of NI to a solution of the $CsPbBr_3$ NCs gives rise to virtually no quenching of the emission intensity or lifetime (Fig. S5).

Figure 1c-e show that $CsPbBr_3$ and $CsPbBr_3$-NI-1 nanoparticles have identical morphology, indicating that addition of NI-1 does not affect the nanoparticle's structure. According to transmission electron microscopy (TEM), the particles appear as cubic structures with average size (the dimension along a side) of ~9 nm for both the $CsPbBr_3$ and the $CsPbBr_3$-NI-1 hybrid. The high-resolution TEM images in Figure 1d and 1f reveal that the NCs are highly crystalline. Figure 1d shows the lattice fringes of $CsPbBr_3$ is 2.92 Å, which corresponds to the (200) facet of the cubic $CsPbBr_3$.[26] After addition of NI-1, Figure 1f emphasized the well-aligned crystalline structure for the $CsPbBr_3$-NI-1 hybrid with a cubic lattice parameter of 2.38 Å, which is due to the (211) facet of the cubic $CsPbBr_3$ phase.[26] The XRD results indicates that all $CsPbBr_3$-NI-n samples crystallized in cubic phase (Figure S6, ESI†). In summary, after being combined with NI-1, the photoluminescence of $CsPbBr_3$ NCs was significantly quenched, but the surface adsorbed imide quencher does not affect the NC morphology and crystal structure.[25,27]

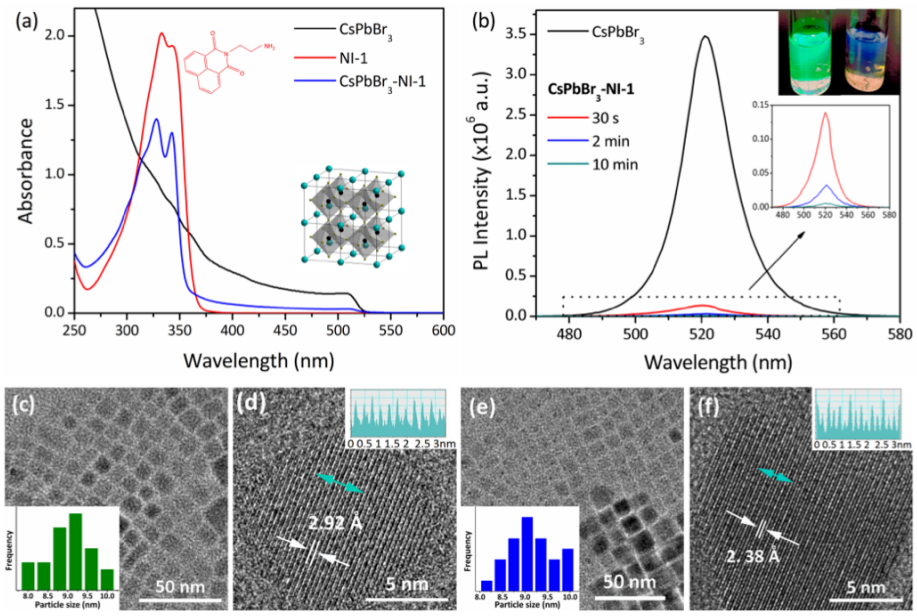

Figure 1. (a) Steady-state absorption spectra of $CsPbBr_3$ NCs, NI-1, and $CsPbBr_3$-NI-1 hybrid samples. (b) PL evolution of $CsPbBr_3$ NCs after adding NI-1. The excitation wavelength was 400 nm. The photo in (b) shows the images of $CsPbBr_3$ NCs (left) and $CsPbBr_3$-NI-1 hybrid sample (right) under 365 nm UV light. TEM and HRTEM images of $CsPbBr_3$ NCs (c, d) and $CsPbBr_3$-NI-1 hybrid sample (e, f). The insets in c, e showed the size distribution according to TEM observation. The insets in d, f show the profile of lattice fringes in green arrow areas.

Steady state emission measurements indicate that there is efficient PL quenching induced by addition of NI-1 to the $CsPbBr_3$ NCs. To obtain insight into the mechanism for the quenching process, femtosecond-picosecond transient absorption (TA) experiments were performed. The excitation wavelength was at 400 nm to ensure selective photoexcitation of $CsPbBr_3$ and that NI-1 is not excited. As shown in Figure 2a-c, TA spectra were recorded for $CsPbBr_3$ and $CsPbBr_3$-NI-1.

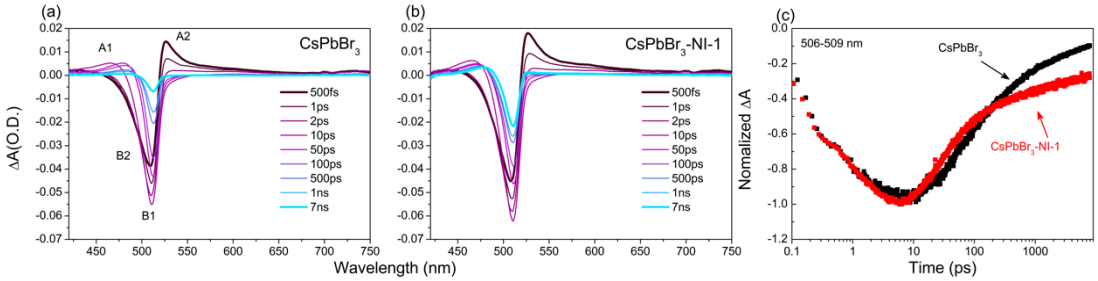

Figure 2. TA spectra of $CsPbBr_3$ (a) and $CsPbBr_3$-NI-1 (b). Excitation wavelength is 400 nm for both samples and the $CsPbBr_3$ NC concentration is 1.54 μM. The spectra were recorded from 500 fs to 7 ns delay. (c) Normalized bleach recovery kinetic

traces of $CsPbBr_3$ NCs and $CsPbBr_3$-NI-1 sample recorded at 506-509 nm on a 7000 ps time scale.

The spectra for the two samples are qualitatively similar, with some notable exceptions described below. (The reader is referred to the following references for the transient absorption typical of $CsPbBr_3$ nanoparticles.)[12,28-30] In particular, the spectra of both samples feature transient absorption (A_1 and A_2) to the blue and red of the bleach due to absorption to higher excitonic states. The spectra are dominated by the negative feature (B_2 and B_1), which is attributed to a superposition of the bleach of the ground state absorption and stimulated emission.[12,30] Close comparison of the spectra in Fig. 2a and 2b reveals that for $CsPbBr_3$-NI the negative absorption feature persists to much longer timescale than for $CsPbBr_3$.[12] At the longest delay time (7 ns), ~35% of the negative absorption remains for $CsPbBr_3$-NI-1, whereas for the control sample the negative absorption has decayed to ~10% of its initial amplitude. In addition, on the short wavelength side of the bleach (~460 nm), there is a pronounced positive absorption that persists at 7 ns for $CsPbBr_3$-NI-1 (Fig. 2b), and a similar feature is not seen in the control (Fig. 2a). The TA dynamics at the maximum of the negative absorption are shown in Fig. 2c. Here it can be seen that the initial decay is more rapid for $CsPbBr_3$-NI, but then at longer times the decay is markedly slower.[12] These features can be seen more quantitively by the comparison of the kinetic fits for the transient absorption in Table S1.

Taken together, we attribute the distinct differences seen in the $CsPbBr_3$-NI sample as arising from a photoinduced electron transfer from $CsPbBr_3$ to the surface anchored naphthalene imide, eq. 2.

$$CsPbBr_3\text{-NI} + h\nu \rightarrow {}^*CsPbBr_3(h\text{-}e)\text{-NI} \quad (1)$$

$${}^*CsPbBr_3(h\text{-}e)\text{-NI} \rightarrow CsPbBr_3(h)\text{-}NI^{-\cdot} \quad (2)$$

$$CsPbBr_3(h)\text{-}NI^{-\cdot} \rightarrow (CsPbBr_3)\text{-}NI \quad (3)$$

The resulting charge separated state decays via charge recombination, eq. 3, and the rate of this process is slower than decay of the exciton state of the $CsPbBr_3$ which explains the persistent negative absorption at long times in the TA. In addition, the weak positive absorption seen at ~460 nm may be attributed to the absorption of the reduced state of the imide acceptor ($NI^{-\cdot}$). As can be seen in the Supporting Information, $NI^{-\cdot}$ exhibits a broad, weak absorption centered at approximately 480 nm (Fig. S11).[31] Our observations are further supported by recent studies by Kamat and co-workers who have used transient absorption and emission quenching to investigate the interaction of $CsPbBr_3$ and surface adsorbed methyl viologen (MV^{2+}).[12] In their studies, they observed very similar persistent negative absorption that was attributed to the charge transfer state arising from photoinduced electron transfer from $CsPbBr_3$ to MV^{2+} acceptor.

While the transient absorption spectra do not provide unequivocal evidence for the existence of the charge transfer state, the features outlined above are a strong indication that electron transfer (eq. 2) is occurring. The TA spectra are dominated by the bleach/absorption features due to the $CsPbBr_3$ because the nanoparticles have a 1000-fold larger molar absorptivity compared to that of the reduced acceptor, $NI^{-\cdot}$ (see Fig. S11).[23,31-32] In other TA studies of $CsPbBr_3$ nanoparticles with electron acceptors,[10,12] it is also found that the spectra are dominated by the bleach/absorption of $CsPbBr_3$, with the absorption of the reduced acceptors being negligible due to the large difference in molar absorptivity.

To further probe the interaction of the NI acceptors with $CsPbBr_3$ NCs, Stern-Volmer (SV) quenching studies were carried out by using both steady state PL quenching and time-resolved PL quenching measurements using time-correlated

single photon counting (TCSPC). In the SV experiments the $CsPbBr_3$ NC concentration was 0.04 μM and the concentration of NI-1, -2 and -3 was varied over the range 0 – 2 μM (this corresponds to a ratio of from 0 to 50 NI to $CsPbBr_3$ NC). Figure 3 shows the results of the steady-state quenching (upper panels, Fig. 3a-c) and the lifetime quenching (middle panels, Fig. d-f) for the three different NI quenchers. There are several notable features that can be seen in this data. First, all of the NI acceptors give rise to quenching with the efficiency varying in the sequence NI-1 > NI-2 > NI-3. This result clearly indicates that the length of the linker chain between the amino anchor group and the NI acceptor influences quenching efficiency. Second, the TCSPC traces show quite clearly that the PL lifetime is quenched by addition of the NI quenchers. This result was a surprise, given the expectation that the NI quenchers are believed to be surface attached to the $CsPbBr_3$ NCs, and therefore a static quenching mechanism was expected.

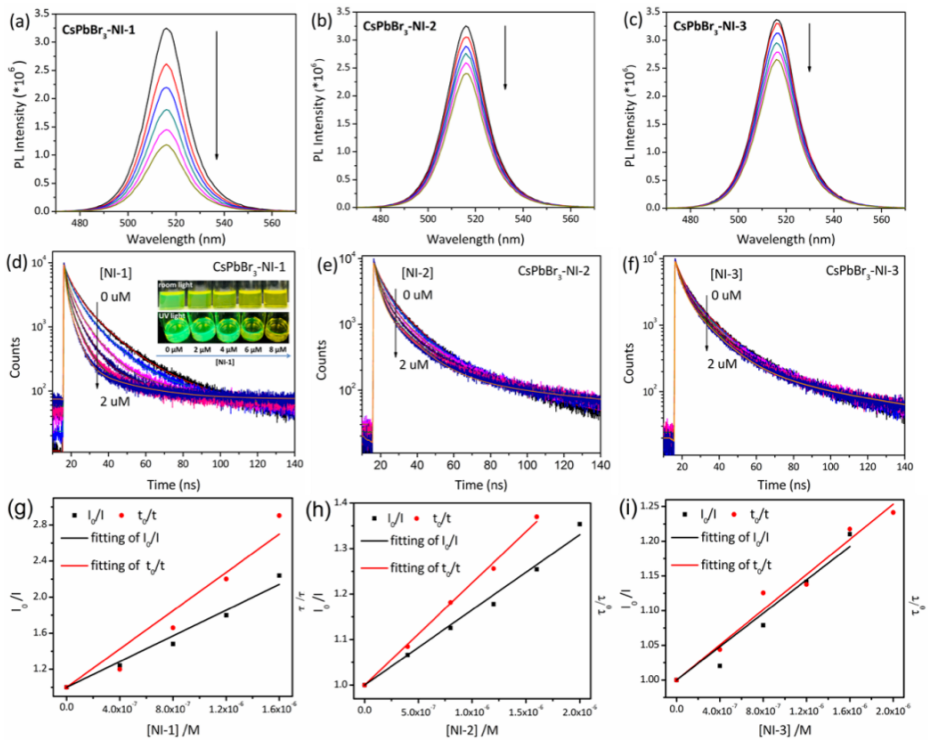

Figure 3. PL quenching of $CsPbBr_3$ NCs with gradual addition of NI-1 (a), NI-2 (b), NI-3 (c). The excitation wavelength was 400 nm. The quenching was indicated by the arrows. Time-resolved PL decay curves of $CsPbBr_3$-NI-1 (d), $CsPbBr_3$-NI-2 (e),

$CsPbBr_3$-NI-3 (f). The concentration of NI-1/NI-2/NI-3 was increased from 0 uM to 2 uM. Inset in (d) shows a color image of $CsPbBr_3$ NC solution with the concentration of NI-1 increased from 0 to 8 μM under room light and 365 nm UV light. (g-i) The Stern-Volmer plots for NI-1, NI-2 and NI-3. Average decay lifetimes were used for the lifetime quenching plots (see Table S2).

The PL quenching data was analyzed by using the Stern-Volmer equation,

$$\frac{I_0}{\mathrm{I}} = \frac{\tau_0}{\tau} = 1 + K_{\mathrm{sv}}[\mathrm{NI}] \quad (4a)$$

$$K_{sv} = k_q \tau^0 \quad (4b)$$

where, I_o and I, τ_0 and τ are the PL intensities and the average lifetime before and after the addition of NI-n, respectively, K_{SV} is the SV quenching constant, [NI] is the concentration of the NI-n quencher, and k_q is the bimolecular quenching rate constant. The SV plots for all three NI quenchers are shown in Fig. 3g-i. Although there is scatter in the data, the plots are qualitatively linear, and most important the general quenching efficiency for lifetime and steady-state quenching are comparable.

In the classical interpretation of SV quenching, the results imply that the majority of the quenching occurs by a "dynamic" pathway, where the quenching rate is limited by diffusion or the intrinsic rate of the (heterogeneous) electron transfer step. By using the slopes of the SV plots in Fig. 3 the quenching constants (K_{SV}) were determined and are shown in Fig. 4. The values range from ~10^6 M^{-1} for NI-1 to 10^5 M^{-1} for NI-3; calculation of the quenching rate constants reveals quenching rates ranging from k_q = 10^{13} - 10^{12} $M^{-1}s^{-1}$. These rates are clearly well above the diffusion-control limit (~10^{10} $M^{-1}s^{-1}$), pointing to an unusual quenching mechanism given the correspondence of the lifetime and steady state quenching correlations. As an additional test of the quenching mechanism, steady-state PL quenching experiments of $CsPbBr_3$ NCs at lower and higher concentrations (0.008 and 0.2 μM, Fig. S7) were conduced. Here it was seen that there was a slight decrease in the

quenching efficiency at higher NC concentration, but it was less than expected if the mechanism occurs by a classic static pathway, where the quencher-emitter complex concentration would be strongly affected by concentration.

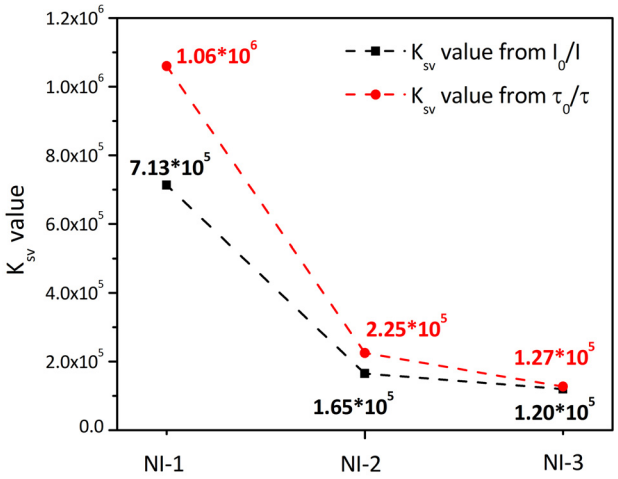

Figure 4. Stern-Volmer quenching constants (K_{SV}) for NI-1, NI-2 and NI-3. Units on K_{SV} are M^{-1}.

General Discussion

The results presented here provide definitive evidence that addition of an amino-functional naphthalene acceptor to $CsPbBr_3$ nanocrystals leads to efficient quenching of the NC exciton. The available evidence supports a photoinduced electron transfer mechanism between the $CsPbBr_3$ exciton and the NI acceptor. By using UPS spectroscopy (Figs. S8 and S9), the frontier energy levels for the $CsPbBr_3$ NCs and the NI acceptors were estimated, and these are shown schematically in Figure 5. Here it can be seen that the LUMO of the NI acceptor lies ~1 eV below the conduction band level of the $CsPbBr_3$ NCs. This offset indicates that interfacial photoinduced electron transfer from the NC to the NI acceptor is quite exothermic and is expected to occur at a relatively high rate. While the fact that electron transfer is exothermic is not proof of the quenching mechanism, quenching via singlet-singlet (Förster) energy transfer can be ruled out (the S_1 state of NI is higher than the

$CsPbBr_3$ exciton level). Furthermore, while Dexter (triplet) energy transfer is possible,[25] electron transfer is typically faster than energy transfer at equal donor-acceptor separation distance.[33]

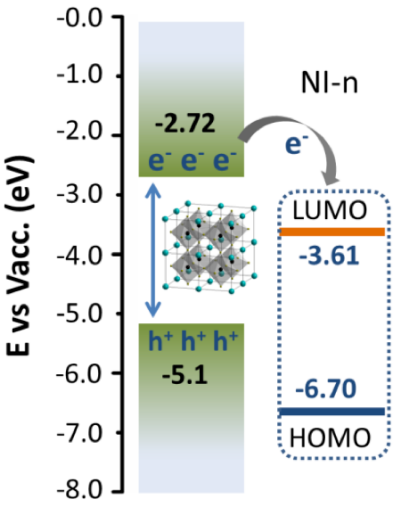

Figure 5. Energy band alignment of $CsPbBr_3$ and NI acceptors.

One interesting result is the observation that the quenching rate decreases substantially with the increasing length of the spacer between the $-NH_2$ anchoring group and the NI acceptor unit. This indicates that the electron transfer rate (eq. 2) is strongly affected by the distance between the NC surface and the acceptor unit, presumably due to a decrease in electronic coupling. The SV results suggest that the rate decreases by a factor of ~10 when the spacer length is increased by 6 $-CH_2-$ units. A similar decrease of rate has been observed in studies of molecular donor-acceptor dyads where the units are separated by flexible tethers of varying length.[34] This suggests that the electronic coupling between the NC surface and the NI acceptor varies with distance in a manner similar to that for molecular electron donor-acceptor systems.[35]

Scheme 1

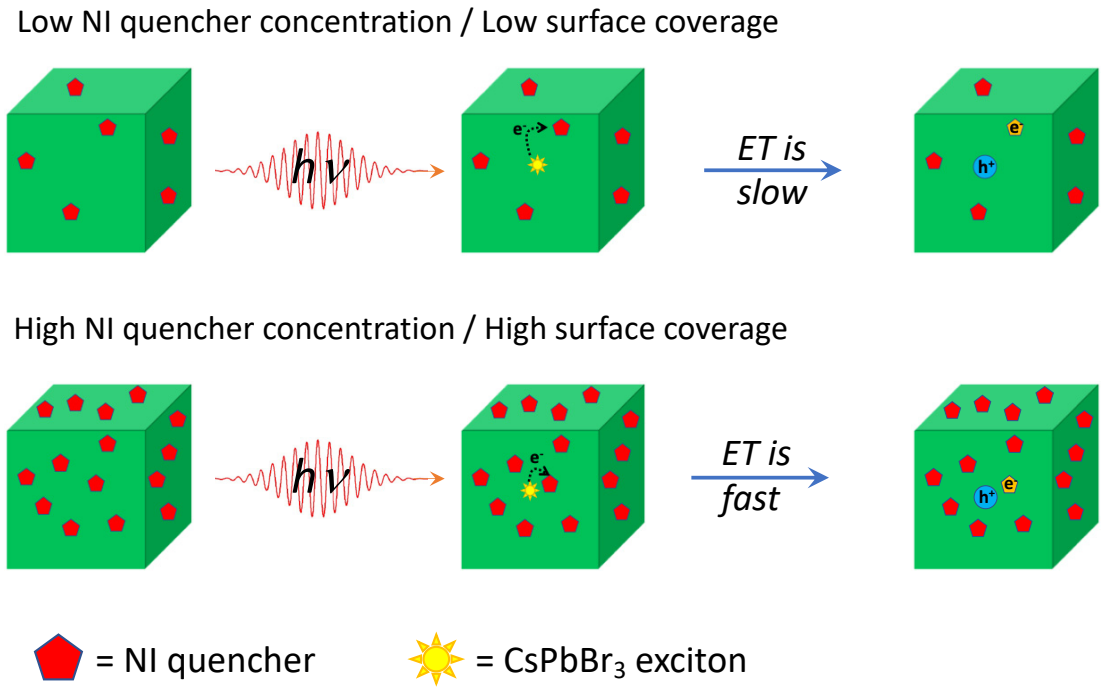

The photoluminescence lifetime quenching experiments clearly show that the $CsPbBr_3$/NI system exhibits dynamic quenching behavior.[36] However, as noted above, the apparent bimolecular rate constants that are derived from the SV results are considerably larger than expected if the quenching is controlled by diffusion of the NI quencher to the excited NC. First, it is important to point out that the mechanism of quenching involves the interaction between the $CsPbBr_3$ exciton and surface bound NI quencher molecules. Therefore, the rates derived from the SV analysis are higher than the diffusion limit because the effective concentration of the quencher is considerably higher than it would be if it is dissolved in homogeneous solution. As shown in Scheme 1, the rate of quenching is expected to vary with the surface concentration of the NI quencher. At low NI concentration, the surface concentration of the quencher is relatively low. Under these conditions, a trapped $CsPbBr_3$ exciton will likely not be in close proximity to a quencher and the rate will be slow. By contrast, at higher NI concentration, the surface concentration of the

quencher will be higher, and the quenching rate will be higher due to the smaller average distance between the exciton and the quencher. As a result, the excition lifetime will vary with quencher (surface) concentration as is observed experimentally (Fig. 3d-f). Similar dynamic quenching of $CsPbBr_3$ NCs by MV^{2+} acceptor was observed in previous studies, but the origin of effect was not noted.[11-12] Other, more detailed studies of CdS quenching by electron acceptors, including MV^{2+}, have exhibited dynamic quenching, and the mechanism is attributed to an acceptor surface concentration dependent rate of interfacial electron transfer.[37-40] While more detailed insight must await further studies, it is evident that the NC to acceptor electron transfer kinetics are first-order in the acceptor surface concentration. Given the observation that the linker length and acceptor surface concentration both influence the rate, it is likely that the interfacial electron transfer step is rate determining.

Summary and Conclusions

The luminescent exciton state of $CsPbBr_3$ NCs is efficiently quenched by addition of amino ($-NH_2$) functionalized naphthalene imide (NI) acceptors. The presence of the amino group is essential to give rise to the quenching and thus it is inferred that the NI acceptors are surface bound to the NC via specific chemical interaction of the amino (or protonated amino) group and the $CsPbBr_3$ interface. The PL quenching is attributed to a photoinduced electron transfer process, where the excited $CsPbBr_3$ transfers an electron to the NI acceptor. Transient absorption spectroscopy gives indirect evidence for the electron transfer step. The efficiency of the quenching varies strongly with the length of the polymethylene spacer between the NI moiety and the NH_2 group. This suggests that the rate of the interfacial electron transfer reaction is (strongly) distance dependent, in much the same way that

the rate of electron transfer decreases (exponentially) with distance between molecular electron donor-acceptor pairs. Time resolved PL quenching experiments reveal that the quenching is a dynamic process, with the rate varying with the surface concentration of the acceptor. The results are interpreted as suggesting that the rate of interfacial electron transfer from the exciton state and the surface bound acceptor is rate determining.

Conflicts of interest

The authors declare no conflict of interest.

Acknowledgements

Dr M. Li acknowledges support from the China Scholarship Council (201808370189) for a visiting studentship at the Department of Chemistry, University of Texas at San Antonio. Work at the University of Texas at San Antonio was supported by the National Science Foundation (Grant No. CHE-1904288).

Supporting Information

Additional experimental results and descriptions are provided. Synthesis and characterization of NI acceptors, calculation of $CsPbBr_3$ solution concentrations, photoluminescence quenching by **NI**, XRD characterization of $CsPbBr_3$ nanoparticles, additional Stern-Volmer quenching results, UPS spectra of NI derivatives and $CsPbBr_3$, NMR spectra of $CsPbBr_3$/**NI-1** hybrid.

This information is available free via the internet at http://pubs.acs.org.

References

1. Protesescu, L.; Yakunin, S.; Bodnarchuk, M. I.; Krieg, F.; Caputo, R.; Hendon, C. H.; Yang, R. X.; Walsh, A.; Kovalenko, M. V. Nanocrystals of Cesium Lead Halide Perovskites ($CsPbBr_3$, X = Cl, Br, and I): Novel Optoelectronic Materials Showing Bright Emission with Wide Color Gamut. *Nano Letters* **2015,** *15*, 3692-3696.

2. Amgar, D.; Aharon, S.; Etgar, L. Inorganic and Hybrid Organo-Metal Perovskite Nanostructures: Synthesis, Properties, and Applications. *Adv. Funct. Mater.* **2016,** *26*, 8576-8593.

3. Song, J.; Li, J.; Li, X.; Xu, L.; Dong, Y.; Zeng, H. Quantum Dot Light-Emitting Diodes Based on Inorganic Perovskite Cesium Lead Halides ($CsPbBr_3$). *Adv. Mater.* **2015,** *27*, 7162-7167.

4. Ho-Baillie, A.; Zhang, M.; Lau, C. F. J.; Ma, F.-J.; Huang, S. Untapped Potentials of Inorganic Metal Halide Perovskite Solar Cells. *Joule* **2019,** *3*, 938-955.

5. Ahmed, G. H.; Liu, J.; Parida, M. R.; Murali, B.; Bose, R.; AlYami, N. M.; Hedhili, M. N.; Peng, W.; Pan, J.; Besong, T. M. D.; et. al. Shape-Tunable Charge Carrier Dynamics at the Interfaces between Perovskite Nanocrystals and Molecular Acceptors. *J. Phys. Chem. Lett.* **2016,** *7*, 3913-3919.

6. Li, J.; Xu, L.; Wang, T.; Song, J.; Chen, J.; Xue, J.; Dong, Y.; Cai, B.; Shan, Q.; Han, B.; Zeng, H. 50-Fold Eqe Improvement up to 6.27% of Solution-Processed All-Inorganic Perovskite Cspbbr3 Qleds Via Surface Ligand Density Control. *Adv. Mater.* **2017,** *29*, 1603885.

7. Zhao, L.; Lin, Y. L.; Kim, H.; Giebink, N. C.; Rand, B. P. Donor/Acceptor Charge-Transfer States at Two-Dimensional Metal Halide Perovskite and Organic Semiconductor Interfaces. *ACS Energy Lett.* **2018,** *3*, 2708-2712.

8. Zhu, R.; Gao, C.; Sun, T.; Shen, L.; Sun, D.; Li, X. Surface Decorating of $CsPbBr_3$ Nanoparticles with the Chemically Adsorbed Perylenetetracarboxylic Diimide. *Langmuir* **2016,** *32*, 3294-3299.

9. Luo, X.; Liang, G.; Han, Y.; Li, Y.; Ding, T.; He, S.; Liu, X.; Wu, K. Triplet Energy Transfer from Perovskite Nanocrystals Mediated by Electron Transfer. *J. Am. Chem. Soc.* **2020,** *142*, 11270-11278.

10. DuBose, J. T.; Kamat, P. V. Probing Perovskite Photocatalysis. Interfacial Electron Transfer between $CsPbBr_3$ and Ferrocene Redox Couple. *J. Phys. Chem. Lett.* **2019,** *10*, 6074-6080.

11. DuBose, J. T.; Kamat, P. V. Surface Chemistry Matters. How Ligands Influence Excited State Interactions between $CsPbBr_3$ and Methyl Viologen. *J. Phys. Chem. C* **2020,** *124*, 12990-12998.

12. Kobosko, S. M.; DuBose, J. T.; Kamat, P. V. Perovskite Photocatalysis. Methyl Viologen Induces Unusually Long-Lived Charge Carrier Separation in $CsPbBr_3$ Nanocrystals. *ACS Energy Lett.* **2020,** *5*, 221-223.

13. Ou, M.; Tu, W.; Yin, S.; Xing, W.; Wu, S.; Wang, H.; Wan, S.; Zhong, Q.; Xu, R. Amino-Assisted Anchoring of $CsPbBr_3$ Perovskite Quantum Dots on Porous G-C_3N_4 for Enhanced Photocatalytic CO_2 Reduction. *Angw. Chem., Int. Ed.* **2018,** *57*, 13570-13574.

14. Duke, R. M.; Veale, E. B.; Pfeffer, F. M.; Kruger, P. E.; Gunnlaugsson, T. Colorimetric and Fluorescent Anion Sensors: An Overview of Recent Developments in the Use of 1,8-Naphthalimide-Based Chemosensors. *Chem. Soc. Rev.* **2010,** *39*, 3936-3953.

15. Al Kobaisi, M.; Bhosale, S. V.; Latham, K.; Raynor, A. M.; Bhosale, S. V. Functional Naphthalene Diimides: Synthesis, Properties, and Applications. *Chem. Rev.* **2016,** *116*, 11685-11796.

16. Coronado, J. L. G.; Martín, E.; Montero, L. A.; Fierro, J. L. G.; de la Vega, J. M. G. Effects of the 3- and 4-Methoxy and Acetamide Substituents and Solvent

Environment on the Electronic Properties of N-Substituted 1,8-Naphthalimide Derivatives. *J. Phys. Chem. A* **2007,** *111*, 9724-9732.

17. Zhang, J.; Zhang, X.; Xiao, H.; Li, G.; Liu, Y.; Li, C.; Huang, H.; Chen, X.; Bo, Z. 1,8-Naphthalimide-Based Planar Small Molecular Acceptor for Organic Solar Cells. *ACS Appl. Mater. Interfaces* **2016,** *8*, 5475-5483.
18. Sivakumar, G.; Bertoni, A. H.; Kim, H.-S.; Marchezi, P. E.; Bernardo, D. R.; Hagfeldt, A.; Grätzel, M.; Zakeeruddin, S. M.; Nogueira, A. F. Design, Synthesis and Characterization of 1,8-Naphthalimide Based Fullerene Derivative as Electron Transport Material for Inverted Perovskite Solar Cells. *Synth. Met.* **2019,** *249*, 25-30.
19. Do, T. T.; Pham, H. D.; Manzhos, S.; Bell, J. M.; Sonar, P. Molecular Engineering Strategy for High Efficiency Fullerene-Free Organic Solar Cells Using Conjugated 1,8-Naphthalimide and Fluorenone Building Blocks. *ACS Appl. Mater. Interfaces* **2017,** *9*, 16967-16976.
20. Kwon, O. K.; Uddin, M. A.; Park, J.-H.; Park, S. K.; Nguyen, T. L.; Woo, H. Y.; Park, S. Y. A High Efficiency Nonfullerene Organic Solar Cell with Optimized Crystalline Organizations. *Adv. Mater.* **2016,** *28*, 910-916.
21. Mo, S.; Meng, Q.; Wan, S.; Su, Z.; Yan, H.; Tang, B. Z.; Yin, M. Tunable Mechanoresponsive Self-Assembly of an Amide-Linked Dyad with Dual Sensitivity of Photochromism and Mechanochromism. *Adv. Funct. Mater.* **2017,** *27*, 1701210.
22. Bullock, J. D.; Valandro, S. R.; Sulicz, A. N.; Zeman, C. J.; Abboud, K. A.; Schanze, K. S. Blue Phosphorescent Trans-N-Heterocyclic Carbene Platinum Acetylides: Dependence on Energy Gap and Conformation. *J. Phys. Chem. A* **2019,** *123*, 9069-9078.

23. De Roo, J.; Ibáñez, M.; Geiregat, P.; Nedelcu, G.; Walravens, W.; Maes, J.; Martins, J. C.; Van Driessche, I.; Kovalenko, M. V.; Hens, Z. Highly Dynamic Ligand Binding and Light Absorption Coefficient of Cesium Lead Bromide Perovskite Nanocrystals. *ACS Nano* **2016,** *10*, 2071-2081.

24. Ravi, V. K.; Santra, P. K.; Joshi, N.; Chugh, J.; Singh, S. K.; Rensmo, H.; Ghosh, P.; Nag, A. Origin of the Substitution Mechanism for the Binding of Organic Ligands on the Surface of $CsPbBr_3$ Perovskite Nanocubes. *J. Phys. Chem. Lett.* **2017,** *8*, 4988-4994.

25. Mase, K.; Okumura, K.; Yanai, N.; Kimizuka, N. Triplet Sensitization by Perovskite Nanocrystals for Photon Upconversion. *Chem. Commun.* **2017,** *53*, 8261-8264.

26. Zhou, L.; Yu, K.; Yang, F.; Cong, H.; Wang, N.; Zheng, J.; Zuo, Y.; Li, C.; Cheng, B.; Wang, Q. Insight into the Effect of Ligand-Exchange on Colloidal Cspbbr3 Perovskite Quantum Dot/Mesoporous-TiO_2 Composite-Based Photodetectors: Much Faster Electron Injection. *J. Mater. Chem. C* **2017,** *5*, 6224-6233.

27. Koscher, B. A.; Swabeck, J. K.; Bronstein, N. D.; Alivisatos, A. P. Essentially Trap-Free $CsPbBr_3$ Colloidal Nanocrystals by Postsynthetic Thiocyanate Surface Treatment. *J. Am. Chem. Soc.* **2017,** *139*, 6566-6569.

28. Mondal, N.; Samanta, A. Complete Ultrafast Charge Carrier Dynamics in Photo-Excited All-Inorganic Perovskite Nanocrystals ($CsPbBr_3$). *Nanoscale* **2017,** *9*, 1878-1885.

29. Mondal, N.; De, A.; Das, S.; Paul, S.; Samanta, A. Ultrafast Carrier Dynamics of Metal Halide Perovskite Nanocrystals and Perovskite-Composites. *Nanoscale* **2019,** *11*, 9796-9818.

30. Butkus, J.; Vashishtha, P.; Chen, K.; Gallaher, J. K.; Prasad, S. K. K.; Metin, D. Z.; Laufersky, G.; Gaston, N.; Halpert, J. E.; Hodgkiss, J. M. The Evolution of Quantum Confinement in $CsPbBr_3$ Perovskite Nanocrystals. *Chem. Mater.* **2017,** *29*, 3644-3652.

31. Gosztola, D.; Niemczyk, M. P.; Svec, W.; Lukas, A. S.; Wasielewski, M. R. Excited Doublet States of Electrochemically Generated Aromatic Imide and Diimide Radical Anions. *J. Phys. Chem. A* **2000,** *104*, 6545-6551.

32. Maes, J.; Balcaen, L.; Drijvers, E.; Zhao, Q.; De Roo, J.; Vantomme, A.; Vanhaecke, F.; Geiregat, P.; Hens, Z., Light Absorption Coefficient of $CsPbBr_3$ Perovskite Nanocrystals. *J. Phys. Chem. Lett.* **2018,** *9*, 3093-3097.

33. Closs, G. L.; Piotrowiak, P.; MacInnis, J. M.; Fleming, G. R. Determination of Long-Distance Intramolecular Triplet Energy-Transfer Rates. Quantitative Comparison with Electron Transfer. *J. Am. Chem. Soc.* **1988,** *110*, 2652-2653.

34. Ryu, C. K.; Wang, R.; Schmehl, R. H.; Ferrere, S.; Ludwikow, M.; Merkert, J. W.; Headford, C. E. L.; Elliott, C. M. Photoinduced Electron Transfer in Linked Ruthenium(II) Diimine-Diquat Complexes: Linkage Dependence. *J. Am. Chem. Soc.* **1992,** *114*, 430-438.

35. Wasielewski, M. R. Photoinduced Electron Transfer in Supramolecular Systems for Artificial Photosynthesis. *Chem. Rev.* **1992,** *92*, 435-461.

36. The term dynamic quenching is used in the classical Stern-Volmer interpretation, where quenching of the steady state emission parallels the quenching of the exciton decay lifetime.

37. Morris-Cohen, A. J.; Frederick, M. T.; Cass, L. C.; Weiss, E. A. Simultaneous Determination of the Adsorption Constant and the Photoinduced Electron

Transfer Rate for a CdS Quantum Dot–Viologen Complex. *J. Am. Chem. Soc.* **2011,** *133*, 10146-10154.

38. Song, N.; Zhu, H.; Jin, S.; Zhan, W.; Lian, T. Poisson-Distributed Electron-Transfer Dynamics from Single Quantum Dots to C60 Molecules. *ACS Nano* **2011,** *5*, 613-621.
39. Leng, H.; Loy, J.; Amin, V.; Weiss, E. A.; Pelton, M. Electron Transfer from Single Semiconductor Nanocrystals to Individual Acceptor Molecules. *ACS Energy Lett.* **2016,** *1*, 9-15.
40. Harris, R. D.; Bettis Homan, S.; Kodaimati, M.; He, C.; Nepomnyashchii, A. B.; Swenson, N. K.; Lian, S.; Calzada, R.; Weiss, E. A. Electronic Processes within Quantum Dot-Molecule Complexes. *Chem. Rev.* **2016,** *116*, 12865-12919.

TOC Graphic